SILICON CARBIDE GRAINS OF TYPE C PROVIDE EVIDENCE FOR THE PRODUCTION OF THE UNSTABLE ISOTOPE ^{32}Si IN SUPERNOVAE

M. PIGNATARI[1,14], E. ZINNER[2], M. G. BERTOLLI[3,14], R. TRAPPITSCH[4,5,14], P. HOPPE[6], T. RAUSCHER[1,7], C. FRYER[8,14],
F. HERWIG[9,10,14], R. HIRSCHI[11,12,14], F. X. TIMMES[10,13,14], AND F.-K. THIELEMANN[1]

[1] Department of Physics, University of Basel, Klingelbergstrasse 82, CH-4056 Basel, Switzerland
[2] Laboratory for Space Sciences and the Physics Department, Washington University, St. Louis, MO 63130, USA
[3] Theoretical Division (T-2), LANL, Los Alamos, NM 87545, USA
[4] Department of the Geophysical Sciences, University of Chicago, Chicago, IL 60637, USA
[5] Chicago Center for Cosmochemistry, University of Chicago, Chicago, IL 60637, USA
[6] Max Planck Institute for Chemistry, Hahn-Meitner-Weg 1, D-55128 Mainz, Germany
[7] Centre for Astrophysics Research, School of Physics, Astronomy and Mathematics, University of Hertfordshire, College Lane, Hatfield AL10 9AB, UK
[8] Computational Physics and Methods (CCS-2), LANL, Los Alamos, NM 87545, USA
[9] Department of Physics and Astronomy, University of Victoria, Victoria, BC, Canada
[10] The Joint Institute for Nuclear Astrophysics, Notre Dame, IN 46556, USA
[11] Keele University, Keele, Staffordshire ST5 5BG, UK
[12] Kavli Institute for the Physics and Mathematics of the Universe (WPI), University of Tokyo, 5-1-5 Kashiwanoha, Kashiwa 277-8583, Japan
[13] School of Earth and Space Exploration, Arizona State University, P.O. Box 871404, Tempe, AZ 85287-1404, USA

ABSTRACT

Carbon-rich grains are observed to condense in the ejecta of recent core-collapse supernovae (SNe) within a year after the explosion. Silicon carbide grains of type X are C-rich grains with isotopic signatures of explosive SN nucleosynthesis have been found in primitive meteorites. Much rarer silicon carbide grains of type C are a special sub-group of SiC grains from SNe. They show peculiar abundance signatures for Si and S, isotopically heavy Si, and isotopically light S, which appear to be in disagreement with model predictions. We propose that C grains are formed mostly from C-rich stellar material exposed to lower SN shock temperatures than the more common type X grains. In this scenario, extreme ^{32}S enrichments observed in C grains may be explained by the presence of short-lived ^{32}Si ($\tau_{1/2} = 153$ yr) in the ejecta, produced by neutron capture processes starting from the stable Si isotopes. No mixing from deeper Si-rich material and/or fractionation of Si from S due to molecular chemistry is needed to explain the ^{32}S enrichments. The abundance of ^{32}Si in the grains can provide constraints on the neutron density reached during the SN explosion in the C-rich He shell material. The impact of the large uncertainty of the neutron capture cross sections in the ^{32}Si region is discussed.

Key words: stars: abundances – stars: evolution – stars: interiors – stars: massive

Online-only material: color figures

1. INTRODUCTION

Despite recent improvements in simulations of core-collapse supernova (CCSN) explosions (e.g., Janka 2012), the understanding of supernova (SN) still has major gaps, and observations of SN and their ejecta still provide many puzzles (e.g., Fryer et al. 2012 and references therein). Of particular importance may be the asymmetric nature of the explosion and the hydrodynamic development of the layers ejected after the explosion (e.g., Kjær et al. 2010; Isensee et al. 2010; DeLaney et al. 2010).

Several types of presolar grains from primitive carbonaceous meteorites that are associated with SN nucleosynthesis due to their isotopic ratios (see, e.g., Clayton & Nittler 2004; Zinner 2007) provide constraints on these explosions. Presolar grains carry the signatures of their stellar origin, and their interpretation may help to guide CCSN models.

Silicon carbide is one of the types of stardust grains that have been identified in primitive meteorites (e.g., Zinner 2007). While most of these so-called presolar SiC grains originate in asymptotic giant branch stars, there are two rare sub-types of SiC grains that have a CCSN origin. Type X grains (about 1% of all presolar SiC grains) have large excesses in ^{28}Si. This signature

and evidence for the initial presence of ^{44}Ti in a subset of these grains is proof of their SN origin: both isotopes are predicted to be abundant in the Si/S zone of SNe (Rauscher et al. 2002). More recently, Pignatari et al. (2013, hereafter P13), showed that ^{28}Si and ^{44}Ti may also be produced at the bottom of the He shell exposed to high shock velocities and/or high energies, reproducing several isotopic abundance patterns typical of SiC X grains and graphites from SNe.

Silicon carbide grains of type C are even rarer (about 0.1% of all SiC grains) than SiC X grains. They have a large excess in ^{29}Si and ^{30}Si and most of them have been found by automatic searches in the NanoSIMS detection apparatus. Some of these grains contain extinct ^{44}Ti, similar to SiC X grains. Just over a dozen of these grains have been identified, and 9 have been analyzed for their S isotopic ratios, showing large ^{32}S excesses, with ^{32}S/^{33,34}S ratios ranging up to 16 times solar (Amari et al. 1999; Croat et al. 2010; Gyngard et al. 2010; Hoppe et al. 2010, 2012; Zinner et al. 2010; Orthous-Daunay et al. 2012; Xu et al. 2012). This is puzzling because in existing SN models the only zone with large ^{32}S excesses is the Si/S zone (Meyer et al. 1995), which has large ^{28}Si excesses, whereas zones with ^{28}Si depletions (i.e., ^{29,30}Si excesses) are predicted to have also ^{32}S depletions (e.g., Rauscher et al. 2002). Hoppe et al. (2012) have invoked element fractionation between sulfur and silicon by molecule chemistry in the SN ejecta to explain
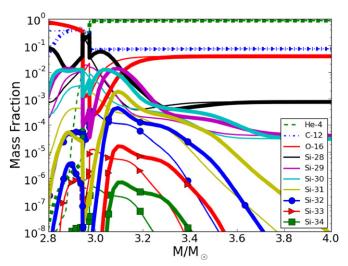

Figure 1. Isotopic abundance profiles given 2.5 s after the explosion in the top of the O/C zone, the C/Si zone, and the He/C zone of the 15 $M_\odot$ SN models 15r and 15r4. Shown are profiles for ^{4}He, ^{12}C, ^{16}O, and the Si isotopes along the neutron capture chain from ^{28}Si to ^{34}Si. The models 15r and 15r4 are represented by thick and thin lines, respectively.

(A color version of this figure is available in the online journal.)

this result. However, this ad hoc explanation cannot explain all the data, especially the S isotopic composition of one C grain with $\delta(^{33}S/^{32}S)$ and $\delta(^{34}S/^{32}S)$ values being as low as -940% (Xu et al. 2012), even more extreme than those of S in the Si/S zone. In this Letter, we propose that the ^{32}S excesses in C grains are due to the radioactive decay of short-lived ^{32}Si ($\tau_{1/2} = 153$ yr; Ouellet & Balraj 2011). We present models of explosive nucleosynthesis in the inner part of the He/C zone, where ^{29}Si and ^{30}Si as well as ^{32}S excesses can be produced while maintaining a C-rich environment.
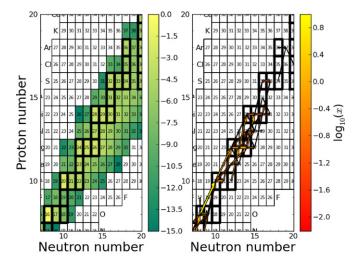
The Letter is organized as follows. In Section 2 we describe the stellar models and the nucleosynthesis calculations, in Section 3 we compare theoretical results with measurements for C grains. Finally, in Section 4 we give our conclusions.

2. STELLAR MODEL CALCULATIONS AND NUCLEOSYNTHESIS

This investigation is based on seven SN explosion models for a 15 $M_\odot$, $Z = 0.02$ star, three of which were introduced in P13. The pre-SN evolution is calculated with the code GENEC (Eggenberger et al. 2008). The explosion simulations include the fallback prescription by Fryer et al. (2012), and are performed for a case with recommended initial shock velocity and six cases where the latter is reduced by a factor of 2, 4, 5, 10, 20, and 100, respectively (models 15r, 15r2, 15r4, 15r5, 15r10, 15r20, and 15r100). The standard initial shock velocity used beyond fallback is 2×10^9 cm s^{-1}. The kinetic explosion energy for these 15 $M_\odot$ models ranges from 4 to 5×10^{51} erg to less than 10^{51} erg. The post-processing code MPPNP is used to calculate the nucleosynthesis in the star before and during the explosion (see, e.g., Bennett et al. 2012). In the present study, we focus only on the C-rich explosive He-burning layers, including the He/C zone and a small part of the O/C zone.

The abundances of key species and $^{28-34}$Si are reported in Figure 1 for models 15r and 15r4. Results are similar for the intermediate model 15r2. The bottom of the He/C zone is strongly affected by the explosion. While ^{12}C is not significantly modified, ^{16}O is depleted and feeds the production of heavier
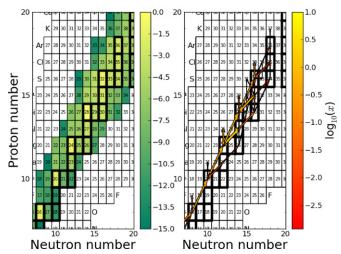

Figure 2. Mass fraction abundance distributions (green, left) and nucleosynthesis fluxes (arrows with red to yellow color, right) at $\sim 10^{-5}$ s (upper panels) and $\sim 10^{-2}$ s (lower panels) after the explosion at mass coordinate 2.95 $M_\odot$ of the model 15r. The nucleosynthesis fluxes, $[\delta Y_i/\delta t]_j$, show the variation of the abundance $Y_i = X_i/A_i$ due to the reaction j. The arrow width and color correspond to the flux strength. Heavy-lined boxes correspond to the stable isotopes.

(A color version of this figure is available in the online journal.)

α-isotopes, including ^{28}Si. This stellar region was defined as the C/Si zone in P13. The main reason for this behavior is the higher α-capture rates starting from the ^{16}O(α, γ)^{20}Ne reaction than that of the ^{12}C(α, γ)^{16}O reaction at explosive He shell temperatures (as explained by P13). Models with lower shock velocities show weaker explosion signatures. In particular, model 15r100 does not show any significant departures from pre-explosive abundances during the explosion in the C-rich region.

Along the Si neutron capture chain, $^{29-30}$Si and heavier unstable Si species are produced efficiently by neutron captures starting from ^{28}Si. The larger explosion temperatures in model 15r than in model 15r4 are pushing the production peaks of different Si neutron-rich species to larger mass coordinates, not significantly affecting their absolute abundance. Therefore, abundance yields for the Si isotopes in the explosive He shell result from the interplay between α-captures and neutron captures, triggered by activation of the ^{22}Ne(α, n)^{25}Mg neutron source (e.g., Meyer et al. 2000 and references therein). The main abundance features and dominating nucleosynthesis fluxes for two different times of the SN explosion are given in Figure 2, in the so-called C/Si zone ($M \sim 2.95$ $M_\odot$, model 15r; see also
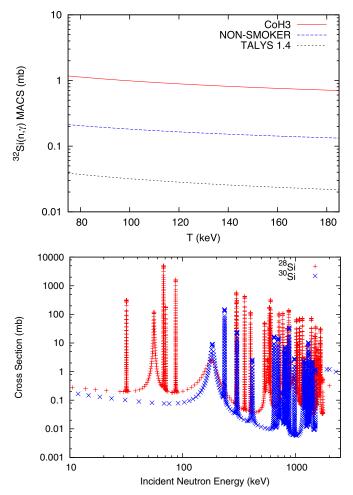
Figure 3. Upper panel: neutron capture MACS for ^{32}Si, calculated by different statistical HF models in the temperature range of interest $T = 1$–2×10^9 K (corresponding to ~90–170 keV). No experimental data exist for ^{32}Si, therefore one has to rely on theoretical calculations. Statistical methods are not applicable in the primary energy range of interest for this nucleus, therefore a more appropriate approach is needed to constrain the uncertainty. Lower panel: neutron capture cross sections for ^{28}Si and ^{30}Si from the ENDF/B-VII.1 library (see the end of Section 2 for discussion).

(A color version of this figure is available in the online journal.)

P13). In the early stages of the explosion, depending on the available ^{22}Ne, the α-capture path starting from ^{16}O is accompanied by $(n, \gamma)(\alpha, n)$ sequences, producing the same α-species. An example is ^{20}Ne$(\alpha, \gamma)^{24}$Mg and ^{20}Ne$(n, \gamma)^{21}$Ne$(\alpha, n)^{24}$Mg. During the later stages of the explosion and/or low ^{22}Ne abundances, the (α, γ) fluxes become dominant. Note that for explosive He-burning conditions the (α, p) fluxes are compensated by their reverse reactions, and proton captures on the abundant α-isotopes do not affect the abundance of their parent species because of the efficient reverse (γ, p) photodisintegrations.

In the present calculations, we use for the (n, γ) reactions on unstable Si species the rates from Hauser–Feshbach (HF) calculations by the NON-SMOKER code (Rauscher & Thielemann 2000), available in JINA REACLIB version 1.1 (e.g., Cyburt et al. 2010). The uncertainties of the neutron capture rates in the mass region of ^{32}Si are very large. Figure 3, upper panel, shows the Maxwellian-averaged cross section (MACS) for neutron capture on ^{32}Si as calculated from the HF codes CoH$_3$ (Kawano et al. 2004) and TALYS 1.4 (Koning et al. 2008, 2011), and NON-SMOKER. At a temperature near 90 keV (~10^9 K), we see a difference of almost two orders of magnitude between the

highest (from CoH$_3$) and the lowest calculated values (TALYS 1.4). Note, however, that these theoretical predictions are still consistent within the large uncertainty of the ^{32}Si$(n, \gamma)^{33}$Si rate. The large uncertainty is due to the nuclear level density being too low to apply the HF model for neutron-rich isotopes of Si. The model relies on the statistical averaging over levels in the compound nucleus and thus a sufficiently high nuclear level density is required at the compound formation energy (Rauscher et al. 1997). The ENDF/B-VII.1 library of Chadwick et al. (2011) provides the location of neutron capture resonances for even–even nuclei near ^{32}Si, as shown in Figure 3, lower panel. While no data are available on ^{32}Si neutron capture resonances, the neighboring even–even nuclei ^{30}Si and ^{28}Si give an indication of the number of levels accessible at different incident particle energies. Above an energy of ~600 keV statistical methods become appropriate. For this reason, we considered an uncertainty of a factor of 100 for the ^{32}Si neutron capture cross section. The impact of this uncertainty is presented in Section 3.

Where experimental knowledge of the single resonances has been obtained, such as in the case of ^{28}Si and ^{30}Si, uncertainties may still arise from the precise location and strength of each resonance. However, uncertainties from experiment are expected to be much lower than those introduced by the use of HF calculations in an inappropriate region.

3. COMPARISON WITH OBSERVATIONS

We compare in Figure 4 the abundances from the C-rich ejecta from our models (Section 2) originating from the C/Si zone, the whole He/C zone, and the C-rich part of the He/N zone, with isotopic ratios of single SiC X and C grains from the St. Louis Presolar Grains Database (Hynes & Gyngard 2009). No mixing between layers is considered and SiC X and C grains with ^{12}C/^{13}C lower than solar are excluded. They are not reproduced by these models that have high C isotopic ratio.

The standard model (15r, upper panel, layer 1 Figure 4) shows a strong ^{28}Si and ^{32}S production and the absence of ^{32}Si in the C/Si zone during the explosion (see also P13). Outward, in the inner part of the He/C zone, the lower explosion temperatures and the neutron burst triggered by the ^{22}Ne$(\alpha, n)^{25}$Mg (n process; e.g., Meyer et al. 2000) gradually reduce ^{28}Si and ^{32}S enrichments, whereas ^{32}Si is synthesized and accumulated according to its neutron capture cross section (as discussed in Section 2). The outer parts of the He/C zone show mild enrichments of the stable neutron-rich Si and S isotopes due to pre-explosive s-processing.

The ^{28}Si excess observed in SiC X grains are reproduced in parts of the C/Si zone for the models 15r and 15r2 (e.g., layer 1 of model 15r, Figure 4, lower panel). SiC C grains show larger ^{32}S excesses than SiC X grains, and positive $\delta(^{30}$Si$)$. Such a signature is consistent with abundance predictions from more external zones in the C-rich He shell. In models 15r4–15r20, the shock temperature is not sufficient to reproduce the ^{28}Si excess observed in SiC X grains (see also P13). Conversely, the presented models can reproduce the Si and S isotopic ratios in the C grains over a large range in initial shock velocities. Also in the case of contamination or mixing with isotopically more normal material (see P13), the grain signatures can be explained since $\delta(^{30}$Si$)$ values up to ~15,000–20,000 (e.g., models 15r, 15r2, and 15r4, zones "2" and "3") are associated with large ^{32}S enrichments ($\delta(^{34}$S$) \sim -1000$, Figure 4, lower panel, outside the plot range). For most of the He shell material, the ^{32}Si signature dominates S isotopic anomalies, assuming an arbitrary Si/S
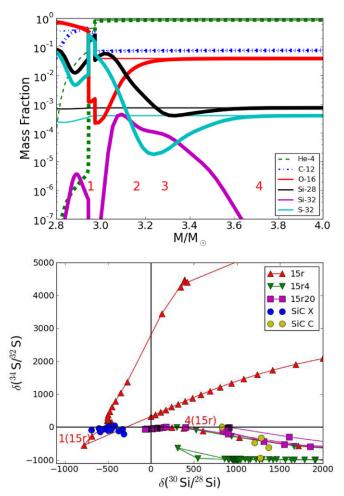
Figure 4. Upper panel: abundances of selected isotopes in the outer part of the O/C zone and the He/C zone for model 15r before and after CCSN explosion (thin and thick lines). Lower panel: the ^{30}Si/^{28}Si and ^{34}S/^{32}S isotopic ratios of presolar SiC X and C grains, plotted as δ-values, deviations from the solar ratios in parts per thousand (‰), are compared with predictions of three different models (15r, 15r4, and 15r20) in the mass range shown in the upper panel. We highlight the predicted Si and S isotopic ratios of model 15r at two different mass coordinates, $M = 2.95$ and $3.7\,M_\odot$ (see upper panel). The Si isotopic ratios of zones "2" and "3" are located out of the plot range, with $\delta(^{30}\text{Si}) \sim 15,000$ and $\delta(^{34}\text{S}) \sim -1000$. A fractionation factor of 10^4 for Si/S is assumed.

(A color version of this figure is available in the online journal.)

Figure 5. Upper panel: final isotopic ratio ^{32}Si/^{28}Si in the C-rich explosive He shell for models with initial shock velocities varying by a factor of 100 (decreasing from model 15r to 15r100). The blue-shaded area denotes O-rich material. For comparison, the red-shaded area indicates the range of ^{32}Si/^{28}Si ratios, inferred from S isotopic ratios and S and Si abundances in presolar SiC C grains, under the assumption that the measured ^{32}S excess derives from ^{32}Si decay. Lower panel: impact on the ^{32}Si/^{28}Si ratio from increasing the ^{32}Si neutron capture cross section by a factor of 100 for models 15r5 and 15r10.

(A color version of this figure is available in the online journal.)

fractionation of 10^4 during grain formation (Figure 4, lower panel). This assumption expresses the hypothesis that all ^{32}S observed in C grains originates from the decay of ^{32}Si (see below for details). Only little S condenses into SiC grains, justifying the assumed elemental fractionation (e.g., Amari et al. 1995).

In Figure 5, upper panel, we show the ^{32}Si/^{28}Si isotopic ratios from different models described in Section 2, comparing them with the ratios inferred for C grains from the radiogenic ^{32}S. We estimated the ratio of the radioactive ^{32}Si (^{32}S*) to ^{28}Si and thus the original ^{32}Si/^{28}Si ratio by assuming that all the S (S$_{\text{tot}}$) in the grains was either ^{32}S* or isotopically normal S (S$_{\text{norm}}$) from contamination. The latter assumption is based on the fact that S is volatile and is not likely to condense into SiC. The grains are therefore expected to contain only marginal intrinsic S. Second, the S concentrations are low in the He shell layers with no ^{28}Si enrichment. Finally, some of the S isotopic images of the C grains measured showed ^{34}S to be more abundant at the edges of the grains and ^{32}S excesses to be higher in interior
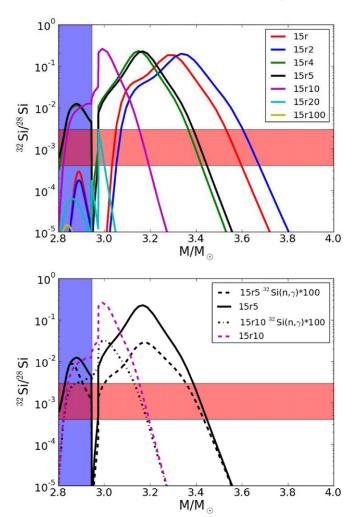
than in border regions. We determined the atomic ^{32}Si/^{28}Si ratios by applying an S$^-$/Si$^-$ sensitivity factor of three, inferred from measurements of Si and S ion yields on synthetic SiC and Mundrabilla FeS, respectively (Hoppe et al. 2012). Since ^{32}S$_{\text{tot}} = ^{32}$S* + ^{32}S$_{\text{norm}}$ and ^{32}S* $= -0.001 \times \delta$S $\times$ (^{32}S* + ^{32}S$_{\text{norm}}$), we obtained the ^{32}S*/^{28}Si ratios by multiplying ^{32}S/^{28}Si with $-0.001 \times \delta$S. Here, ^{32}S$_{\text{norm}}$ is ^{32}S of the isotopically normal component S$_{\text{norm}}$ (assumed to be contamination). For δS, we took the average of $\delta(^{33}\text{S}/^{32}\text{S})$ and $\delta(^{34}\text{S}/^{32}\text{S})$. Within errors the latter two values are equal for all measured grains, providing additional evidence that we are dealing just with an excess in ^{32}Si. In Figure 5, we show that the observed range of ^{32}Si/^{28}Si ratios is matched by predictions from stellar models at different energies, in agreement with Figure 4. Typical conditions required for matching the inferred ^{32}Si/^{28}Si ratios (e.g., at $M = 3.4\,M_\odot$ for models 15r4 and 15r5) have a peak temperature of $\sim 8 \times 10^8$ K and a neutron density peak of $\sim 10^{18-19}$ cm^{-3}, with a ^{28}Si mass fraction of $\sim 5 \times 10^{-4}$. The

models 15r–15r5 with the highest explosion temperatures also fit the observed ^{32}Si/^{28}Si ratio deeper in the He shell (e.g., at $M = 3.05 \, M_\odot$ for models 15r and 15r2), with a ^{28}Si mass fraction of $\sim 5 \times 10^{-2}$. In these cases, the temperature peak is about 1.6×10^9 K, with a neutron density peak of a few 10^{22} cm^{-3} for few 10^{-5} s, dropping quickly to densities more typical of the n process.

Since the grains may contain some normal component (P13), the inferred ^{32}Si/^{28}Si needs to be considered a lower limit of the original ratio in the He shell material. In Figure 5, lower panel, we show that increasing the neutron capture cross section of ^{32}Si by a factor of 100 (see discussion in Section 2) does not change our results. By reducing the ^{32}Si MACS of the same factor the ^{32}Si/^{28}Si ratio increases by less than 10%, since the ^{32}Si MACS adopted in our models is already lower than 1 mb, behaving as a bottleneck in the neutron capture flow feeding heavier Si species. Note that at the temperatures of explosive He burning the half-life of ^{32}Si can be reduced down to few days (e.g., Oda et al. 1994). However, the timescale of the explosive nucleosynthesis is less than ~ 0.3 s, and the impact of the ^{32}Si half-life in the calculations is negligible.

We have shown that CCSN models can explain the large ^{32}S excess measured in SiC C grains by the radioactive decay of the unstable isotope ^{32}Si after grain formation. Furthermore, in SiC C grains most of the remaining S is coming from contamination. We have identified two typical conditions where the correct ^{32}Si/^{28}Si ratio can be obtained, depending on the explosion temperature and on the abundance of ^{28}Si.

4. CONCLUSIONS

We have compared the isotopic signatures in presolar SiC grains of type C with nucleosynthesis predictions for CCSN ejecta exposed to different shock velocities. We propose that the seemingly incompatible Si and S isotopic ratios in these grains are explained by assuming that the ^{32}S excess observed today originates from radioactive ^{32}Si that condensed into the forming SiC grains, and decayed into ^{32}S at later stages. Assuming that all the remaining S is due to contamination, we estimated the ^{32}Si/^{28}Si ratio in the parent CCSN ejecta, ranging from a few 10^{-4} to a few 10^{-3}. We propose this ratio to be a lower limit of its original value in the explosive He shell layers, depending on the level of contamination or mixing with more normal material for each C grain. Such ratios can be produced for different shock velocities and/or explosion energies. Two typical conditions reproducing directly the observed ^{32}Si/^{28}Si ratios are: one with high temperature and large ^{28}Si abundance ($\sim 1.6 \times 10^9$ K and $\sim 5 \times 10^{-2}$, respectively), and the other with temperature ~ 0.7–0.9×10^9 K and ^{28}Si abundance $\sim 5 \times 10^{-4}$. In the first case, the neutron density reaches a peak of a few 10^{22} cm^{-3} for few 10^{-5} s, rapidly dropping to values more typical of the n-process neutron burst. In the second case, the neutron density peak is on the order of 10^{18-19} cm^{-3}.

In conclusion, C grains carry a record of the neutron density reached in the explosive He shell of the CCSN where they formed. We showed that the theoretical nuclear reactions in the ^{32}Si mass region have large uncertainties, but our results are not significantly affected. We conclude that C grains carry the signature of lower energy ejecta compared to SiC X grains, showing positive δ(Si) values and a significant amount of ^{32}Si produced by neutron captures.

REFERENCES

Amari, S., Lewis, R. S., & Anders, E. 1995, GeCoA, 59, 1411
Amari, S., Zinner, E., & Lewis, R. S. 1999, ApJL, 517, L59
Bennett, M. E., Hirschi, R., Pignatari, M., et al. 2012, MNRAS, 420, 3047
Chadwick, M., Herman, M., Obložinský, P., et al. 2011, NDS, 112, 2887
Clayton, D. D., & Nittler, L. R. 2004, ARA&A, 42, 39
Croat, T. K., Stadermann, F. J., & Bernatowicz, T. J. 2010, AJ, 139, 2159
Cyburt, R. H., Amthor, A. M., Ferguson, R., et al. 2010, ApJS, 189, 240
DeLaney, T., Rudnick, L., Stage, M. D., et al. 2010, ApJ, 725, 2038
Eggenberger, P., Meynet, G., Maeder, A., et al. 2008, Ap&SS, 316, 43
Fryer, C. L., Belczynski, K., Wiktorowicz, G., et al. 2012, ApJ, 749, 91
Gyngard, F., Nittler, L. R., & Zinner, E. 2010, M&PSA, 73, 5242
Hoppe, P., Fujiya, W., & Zinner, E. 2012, ApJL, 745, L26
Hoppe, P., Leitner, J., Gröner, E., et al. 2010, ApJ, 719, 1370
Hynes, K. M., & Gyngard, F. 2009, in 40th Lunar and Planetary Institute Science Conference, 1198
Isensee, K., Rudnick, L., DeLaney, T., et al. 2010, ApJ, 725, 2059
Janka, H.-T. 2012, ARNPS, 62, 407
Kawano, T., Chiba, S., Maruyama, T., et al. 2004, in Proc. 2003 Symp. on Nuclear Data, ed. T. Ohsawa & T. Fukahori (Tokai: Japan Atomic Energy Research Institute), 196
Kjær, K., Leibundgut, B., Fransson, C., Jerkstrand, A., & Spyromilio, J. 2010, A&A, 517, A51
Koning, A., Hilaire, S., & Goriely, S. 2011, TALYS-1.4 (Petten, The Netherlands: Nuclear Research and Consultancy Group)
Koning, A. J., Hilaire, S., & Duijvestijn, M. C. 2008, in Proc. Int. Conf. on Nuclear Data for Science and Technology, ed. O. Bersillon, F. Gunsing, E. Bauge, R. Jacqmin, & S. Leray (Les Ulis: EDP Sciences), 211
Meyer, B. S., Clayton, D. D., & The, L.-S. 2000, ApJL, 540, L49
Meyer, B. S., Weaver, T. A., & Woosley, S. E. 1995, Metic, 30, 325
Oda, T., Hino, M., Muto, K., Takahara, M., & Sato, K. 1994, ADNDT, 56, 231
Orthous-Daunay, F.-R., Gyngard, F., Moynier, F., & Zinner, E. 2012, in 43rd Lunar and Planetary Institute Science Conference, 2679
Ouellet, C., & Balraj, B. 2011, NDS, 112, 2199
Pignatari, M., Wiescher, M., Timmes, F. X., et al. 2013, ApJL, 767, L22
Rauscher, T., Heger, A., Hoffman, R. D., & Woosley, S. E. 2002, ApJ, 576, 323
Rauscher, T., & Thielemann, F.-K. 2000, ADNDT, 75, 1
Rauscher, T., Thielemann, F. K., & Kratz, K.-L. 1997, PhRvC, 56, 1613
Xu, Y. C., Amari, S., Gyngard, F., Zinner, E., & Lin, Y. 2012, M&PSA, 47, 5104
Zinner, E. 2007, in Treatise on Geochemistry, Update 1.02, ed. H. D. Holland, K. K. Turekian, & A. Davis (Oxford: Elsevier), 1
Zinner, E., Gyngard, F., & Nittler, L. R. 2010, in 41st Lunar and Planetary Institute Science Conference, 1359